

3D Fluid-Structure Interaction Canine Heart Model with Patch to Quantify Mechanical Conditions for Optimal Myocardium Stem Cell Growth and Tissue Regeneration

Heng Zuo*, Dalin Tang^{*,†,‡}, Chun Yang^{*,§}, Glenn Gaudette[¶], Kristen L. Billiar[¶] and Pedro J. del Nido^{||}

Abstract: Right ventricular (RV) dysfunction is a common cause of heart failure in patients with congenital heart defects and often leads to impaired functional capacity and premature death. Myocardial tissue regeneration techniques are being developed for the potential that viable myocardium may be regenerated to replace scar tissues in the heart or used as patch material in heart surgery. 3D computational RV/LV/Patch models with fluid-structure interactions (FSI) were constructed based on data from a healthy dog heart to obtain local fluid dynamics and structural stress/strain information and identify optimal conditions under which tissue regeneration techniques could achieve best outcome. RV/LV/Patch geometry and blood pressure data were obtained from a dog following established procedures. Four FSI models were used to quantify the influence of different patch materials (Dacron scaffold, treated pericardium) on local environment around the patch area, especially focusing on the thickness and stiffness of the patch. Our results indicated that changes in patch stiffness had little impact on the ejection fraction of the right ventricle because the total patch area was small. However, patch stiffness had huge impact on local RV maximum principal stress (Stress- P_1) and strain (Strain- P_1) around the patch area. Compared to the no-patch model, patch models had increased Stress- P_1 and decreased Strain- P_1 values in the patch area. Softer

* Math Sciences Department, Worcester Polytechnic Institute, Worcester MA 01609, USA.

† School of Biological Science & Medical Engineering Southeast University, Nanjing, 210096, China.

‡ Corresponding author. School of Biological Science & Medical Engineering, Southeast University, Nanjing, 210096, China.

§ Network Technology Research Institute, China United Network Communications Co., Ltd., Beijing, 210029, China.

¶ Department of Biomedical Engineering, Worcester Polytechnic Institute, Worcester, MA 01609, USA.

|| Department of Cardiac Surgery, Children's Hospital Boston, Harvard Medical School, Boston, MA 02115 USA.

patches were associated with greater stress/strain variations. Thinner patch led to complex local flow environment which may have impact on myocytes seeding and RV remodeling. Our multi-physics RV/LV/Patch FSI model can serve as a useful tool to investigate cellular biology and tissue regeneration under localized flow and structural stress environment.

Keywords: Right ventricle, fluid-structure interaction, patch material, myocardium regeneration.

1 Introduction

Right ventricular dysfunction is a common cause of heart failure in patients with congenital heart defects and often leads to impaired functional capacity and premature death [1]. Patients with repaired tetralogy of Fallot (ToF), a congenital heart defect which includes a ventricular septal defect and severe right ventricular outflow obstruction, account for the majority of cases with late onset RV failure. The mechanism of failure is a complex interaction of chronic pulmonary valve regurgitation (present since the original repair), a noncontractile and sometimes aneurysmal RV outflow, ventricular scarring from the incision to remove RV outflow muscle at the original repair, and at times some residual obstruction to RV outflow. The current surgical approach, which includes Pulmonary Valve Replacement (PVR), has yielded mixed results, with many patients seeing little if any improvement in RV function, while in others there is a significant improvement [2,3]. New surgical options including scar tissue reduction and RV remodeling have been proposed in order to improve RV function recovery [1]. The RV remodeling aims mainly to reduce non-contracting scar tissue to improve RV ejection fraction. Another tissue engineering approach was to generate contracting myocardium and use it to replace patch and scar. Tang et al. introduced RV/LV/Patch models to investigate the effects of patch material mechanical properties on RV cardiac function [4]. Patches made of Dacron scaffold, pericardium and contracting myocardium were considered. Their results indicated that patch made of contracting myocardium has promising potential to improve RV function in patients with repaired TOF [4].

It is desirable to have regenerated myocardium tissues for the patches in surgical procedures. Gaudette et al. have been developing techniques for myocardium regeneration and impressive progress has been made [5]. His techniques included seeding stem cells on a patch implanted to a canine heart to promote myocardium regeneration. In this paper, RV/LV/Patch models with fluid-structure interactions (FSI) based on data from a canine patch model were constructed to identify mechanical conditions favorable for myocardium tissue regeneration. Effects of three different patches on RV cardiac function and mechanical conditions were investi-

gated.

2 Data acquisition and computational models

2.1 Canine patch surgery and data acquisition.

In vivo canine surgical procedures were performed by Dr. Gaudette following approved procedures to place a cell-seeded patch to a canine heart. The goal of the experiment was to find out if the stem cells would be able to survive and promote myocardium regeneration. After the heart was exposed, a portion of the posterolateral right ventricular free wall was isolated using a Satinsky clamp. A full thickness portion of myocardium approximately 15 by 10 mm was excised and the full thickness defect would be repaired with stem cell seeded patches (Figure 1). Eight weeks later, the canine was sacrificed and the heart was taken out for cell counts and analysis [5].

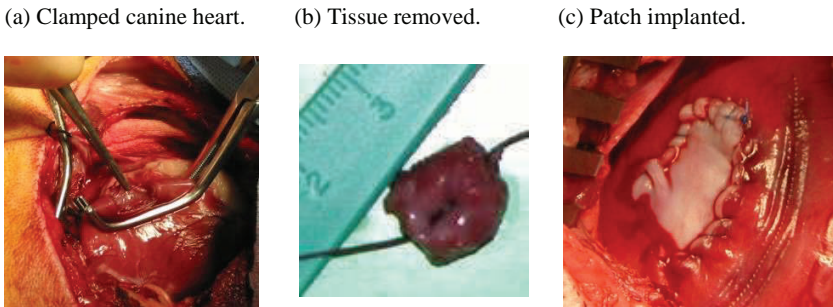


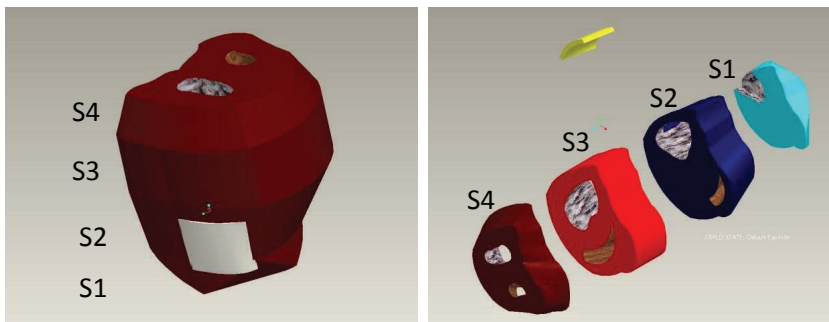
Figure 1: Patch implanting on a canine heart. A full thickness portion of myocardium approximately 15 by 10 mm was excised and a stem cell seeded patch was implanted.

Four sections were obtained from the canine heart for computational model construction. Three-dimensional RV/LV geometry and computational mesh were constructed following the procedures described in [6-9]. Figure 2 shows the 4 original section, corresponding contours and the re-constructed three-dimension RV/LV geometry with patch and valve locations. The re-construction was guided by Dr. Gaudette based on actual surgical observations.

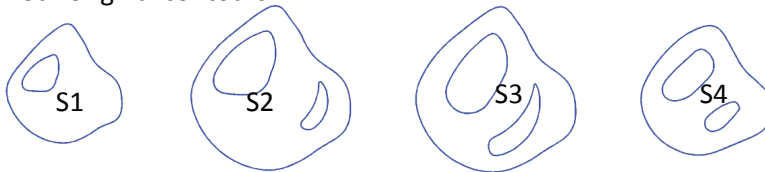
2.2 The RV/LV/Patch model with fluid-structure interactions

Our models included (a) fluid-structure interaction for the right ventricle; (b) passive isotropic material properties; (c) a patch area with different materials and thickness; (d) a structure-only LV as support to the RV structure. Two patch materials

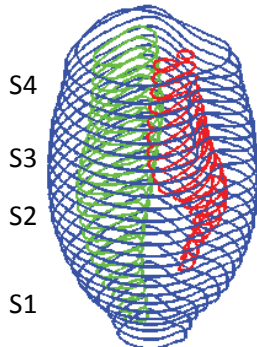
(a) Original 4 sections



(b) Four original contours



(c) 3D RV/LV Geometry with Stacked Contours



(c) 3D RV/LV Geometry with Patch

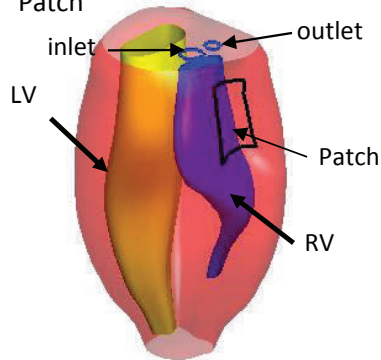


Figure 2: 3D re-construction procedure. (a) Four canine heart sections obtained from surgery; (b) Four original contours; (c) 3D RV/LV Geometry with Stacked Contours; (d) 3D Reconstructed Geometry with Patch.

were considered: Patch 1 - Dacron scaffold; Patch 2 - pericardium, usually from the patient, treated with glutaraldehyde to crosslink the collagen and make it stiffer; and two different thickness were included: 0.5 mm and 1 mm which were much thinner than the original myocardium (average thickness: 10 mm). The 3D CMR-based RV/LV/Patch FSI models were solved to obtain 3D ventricular deformation, local

patch area contraction ratio, and stress/strain distributions for accurate assessment of RV cardiac function and mechanical conditions.

The computational models were used to assess the effect of patch stiffness and thickness with the ultimate goal of finding out optimal patch design and location for myocardium regeneration.

Solid model. The RV, LV and patch materials were assumed to be hyperelastic, isotropic, nearly-incompressible and homogeneous. The governing equations for the structure models are:

$$\rho \frac{\partial^2 u_i}{\partial t^2} = \frac{\partial \sigma_{ij}}{\partial x_j}, \quad i = 1, 2, 3 \quad (1)$$

$$\epsilon_{ij} = \frac{1}{2} \left(\frac{\partial u_j}{\partial a_i} + \frac{\partial u_i}{\partial a_j} + \sum_l \frac{\partial u_l}{\partial a_i} \frac{\partial u_l}{\partial a_j} \right), \quad i, j = 1, 2, 3 \quad (2)$$

Here σ is the stress tensor, ϵ is Green's strain tensor, u is the displacement, and ρ is material density. The nonlinear Mooney-Rivlin model was used to describe the nonlinear properties of the materials with parameter values chosen to match available experimental data and adjusted to reflect stiffness variation of different materials [10,11]. The strain energy function for the modified Mooney-Rivlin model is given by [8,9,10,12,13]

$$W = c_1 (I_1 - 3) + c_2 (I_2 - 3) + D_1 [\exp(D_2 (I_1 - 3)) - 1] \quad (3)$$

$$I_1 = \sum_{ii}^C, \quad I_2 = \frac{1}{2} [I_i^2 - C_{ij}C_{ij}] \quad (4)$$

where I_1 and I_2 are the first and second strain invariants, $C = [C_{ij}] = X^T X$ is the right Cauchy-

Green deformation tensor, $X = [X_{ij}] = [\partial x_i / \partial a_j]$, and c_i and D_i are material parameters chosen to match experimental measurements [10,11]. Several types of patch material with different degrees of elasticity are commercially available in the industry (Dacron, teflon, bovine pericardium, autologous pericardium, etc.). In this paper, we chose two different materials as our patch materials, one is Dacron and the other is treated pericardium. Parameter values for different materials are summarized in Table 1. Material parameters can be adjusted as needed to reflect actual available patch materials and regenerated myocardium. Stress-Stretch curves of normal myocardium, Dacron and treated pericardium are given in Fig 3.

Fluid model. Blood flow was assumed to be laminar, Newtonian, viscous, and incompressible. The Navier-Stokes equations with arbitrary Lagrangian-Eulerian (ALE) formulation were used as the governing equations. Pressure conditions were

Table 1: Parameter values for the patch materials in the RV/LV/Patch material models.

Tissue	c_1 (kPa)	c_2	D_1 (kPa)	D_2
Normal myocardium	2.76	0.0	1.08	2.0
Dacron Scaffold	6×10^3	0.0	3×10^3	1.4
Treated pericardium	13.26	0.0	13.26	9.0

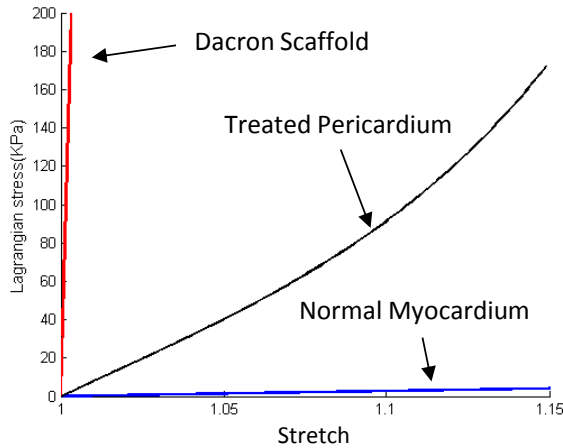


Figure 3: Material stress-stretch curves for ventricular tissue and patch materials.

prescribed at the tricuspid (inlet) and pulmonary (outlet) valves [14]. Since RV muscle was treated as a passive material, pressure conditions were modified so that RV could be inflated properly by fluid forces. No-slip boundary conditions and natural force boundary conditions were specified at all interfaces to couple fluid and structure models together [12,13]. Putting these together, we have

$$\nabla \cdot \mathbf{v} = 0 \quad (5)$$

$$\rho(\partial \mathbf{v} / \partial t + ((\mathbf{v} - \mathbf{v}_g) \cdot \nabla) \mathbf{v}) = \nabla p + \mu \nabla^2 \mathbf{v} \quad (6)$$

$$\mathbf{v}|_{\Gamma} = \frac{\partial x}{\partial t}, \quad \frac{\partial \mathbf{v}}{\partial n}|_{inlet, outlet} = 0 \quad (7)$$

$$P_{inlet} = P_{in}(t) \text{ (inlet open)}, \quad v_{inlet} = 0 \text{ (inlet closed)} \quad (8)$$

$$P_{outlet} = P_{RV}(t) \text{ (outlet open)}, \quad v_{outlet} = 0 \text{ (outlet closed)} \quad (9)$$

$$P|_{LV} = P_{LV}(t) \quad (10)$$

$$\sigma_{ij} \cdot n_j|_{out_wall} = 0 \quad (11)$$

$$\sigma_{ij}^r \cdot n_j|_{interface} = \sigma_{ij}^s \cdot n_j|_{interface} \quad (12)$$

where \mathbf{v} and p are fluid velocity and pressure, \mathbf{v}_g is mesh velocity, μ is blood viscosity, and σ is structure stress tensor (superscripts r and s indicate different materials: fluid, RV tissue, scar, and patch). Together with Eqs. (1)–(10), we have the completed FSI model.

For the sake of simplicity, the cardiac cycle was split into two phases: (a) the filling phase when blood flows in and fills the RV: the inlet was kept open, and the outlet was closed; and (b) the ejection phase when blood was ejected out of RV, the outlet was kept open, and the inlet was closed. When the inlet or outlet was closed, flow velocity was set to zero and pressure was left unspecified. We start our simulation cycle when RV has its smallest volume (end of systole) corresponding to the minimal inlet pressure. As the inlet pressure increases, blood flows into RV and its volume increases. When RV reaches its maximal volume, the inlet closes and the outlet opens. Blood is ejected and RV volume decreases. That completes the cycle. While the mechanism driving the motion is different from the real active contracting heart, our simulated RV motion, deformation, volume change, and fluid flow can provide results matching patient-specific RV volume data with properly adjusted material parameters.

LV model. For simplicity, LV was included as a structure-only model with the same material parameter values used for both LV and RV tissues. A recorded LV pressure was specified inside the LV so that the LV would expand and contract properly matching CMR data. The inclusion of LV is important to obtain the correct RV motion and deformation. Blood flow in the LV was not included to reduce the computational effort.

2.3 Numerical models and solution methods

In this paper, four FSI models were built to investigate the influence of the different patches on flow and LV stress/strain conditions. The details of the four models are listed in Table 2.

Equations (1)–(14) gave the full RV/LV/Patch FSI model which was solved by ADINA (ADINA R&D, Watertown, MA, USA) using unstructured finite elements and the Newton-Raphson iteration method [13,15]. ADINA uses nonlinear incremental iterative procedures to handle fluid-structure interactions. ADINA has been tested by hundreds of real-life applications and has been used by Tang et al. to solve many FSI models. Details for the models and solutions methods are given in [9,13,15].

Table 2: Features of the 4 models used in this paper.

Model Names	Type	Patch	Thickness of Patch(mm)	Patch Material
F0	FSI	No	—	—
F1	FSI	Yes	0.5	Dacron Scaffold
F2	FSI	Yes	0.5	treated pericardium
F3	FSI	Yes	1.0	Dacron Scaffold

3 Results

Four FSI models were solved to obtain stress, strain and flow shear stress information and investigate the impact of different patch designs and the mechanical environment around patch area affecting myocardium regeneration. RV cardiac functions (SV, EF) were also compared among these FSI models.

3.1 Baseline solutions from the RV/LV FSI model without patch

We started from a healthy case (without patch, F0) to gain some baseline information. The fully coupled FSI model was solved by ADINA (ADINA R&D, Waltham, MA) to obtain full 3D flow, deformation, and stress-strain distributions, which would be served as the basis for our investigations. A cut surface was chosen to present stress, strain, and flow behaviors on the RV inner surface. Figure 4 shows the position of the cut surface. Figure 5 presents maximum principal stress (Stress- P_1) and maximum principal strain (Strain- P_1) plots on the RV inner surface at the time when pressure is maximal and minimal. Locations of maximum Stress- P_1 /Strain- P_1 values were observed. RV stress/strain distributions were smooth around the area where a patch would be made. Figure 6 gives four flow velocity plots at different fillings and ejection times, which show interesting patterns with a major vortex. Figure 7 shows flow shear stress distributions in RV at the time of maximal/minimal pressure (P_{max} and P_{min}). These complex flow velocity and shear stress pattern may have a huge impact on patch decision.

3.2 Stress/strain conditions from the patched RV/LV FSI models

Three patched models were constructed and solved for patch comparison and cardiac function analysis: Model 1 (F1) consisted of a Dacron scaffold patch with 0.5mm thickness; Model 2 (F2) consisted of pericardium patch with 0.5mm thickness; and Model 3(F3) consisted of Dacron scaffold patch with 1mm thickness. Figures 8 & 9 present band plots of Stress- P_1 and Strain- P_1 corresponding to maxi-

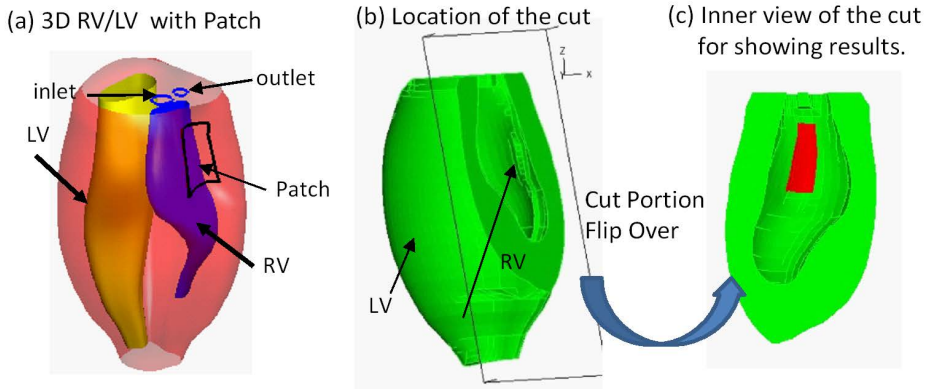


Figure 4: A selected cut-surface for showing stress, strain distribution around patch area from inner view.

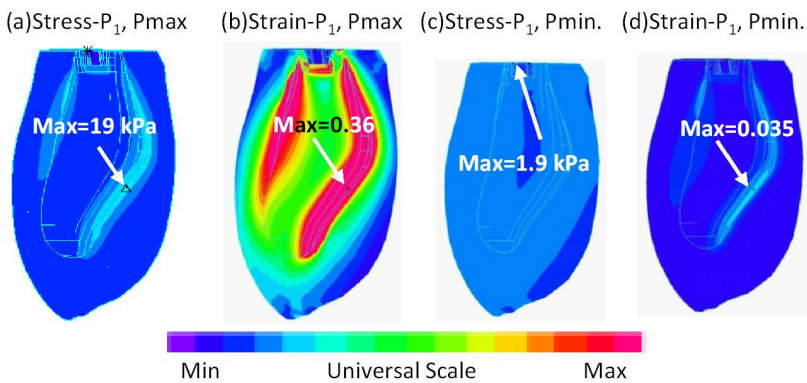


Figure 5: Strain- P_1 and Stress- P_1 distribution on the inner surface at Pmax and Pmin for F0 showing a smooth map of strain/stress at corresponding patch area.

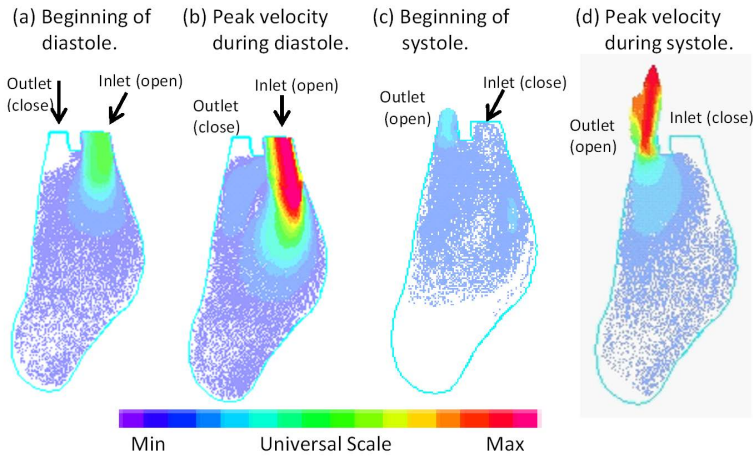


Figure 6: Velocity plots for F0 on a cut surface at different phases showing interesting flow patterns. (a) Beginning of Diastole $t=0.02s$, (b) Peak Velocity during diastole $t=0.24s$, (c) Beginning of Systole $t=0.36s$, (d) Peak Velocity during systole $t=0.44s$.

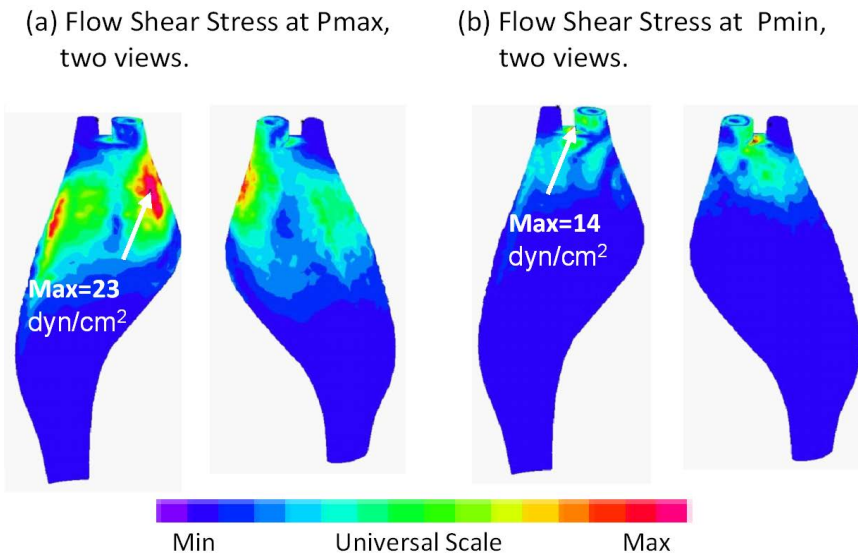


Figure 7: Plots of shear stress distribution for F0 in RV at the time when Pressure is maximal and minimal. Unit for shear stress: dyn/cm^2 .

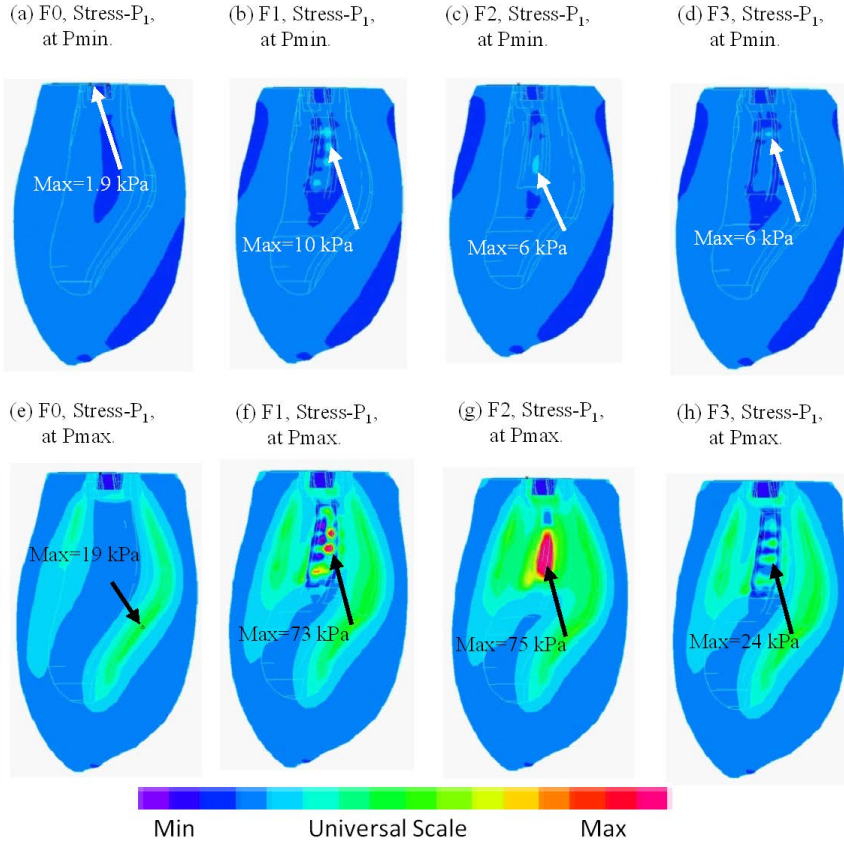


Figure 8: Model comparisons: Stress- P_1 distributions obtained from the patched FSI models showing that the local maximum of Stress- P_1 appears on the patch area and unsmooth distributions happened on the patch area.

imum and minimal pressure conditions to give an overall view of the stress distributions for patched models. Unlike F0 model which had smooth stress distributions, all three patch models had unsmooth distributions on the patch area where the overall maximum of Stress- P_1 appears. Maps of F1 and F3 indicate that the same patch material will lead to similar stress distribution but different thickness of the patch will bring about higher stress values. Maps of F1 and F2 show that different patch material will produce different stress distributions. Maximum of Stress- P_1 /Strain- P_1 for the four FSI models at the time of maximal pressure are summarized in the Table 3.

To obtain more specific information caused by the patch differences, 5 locations

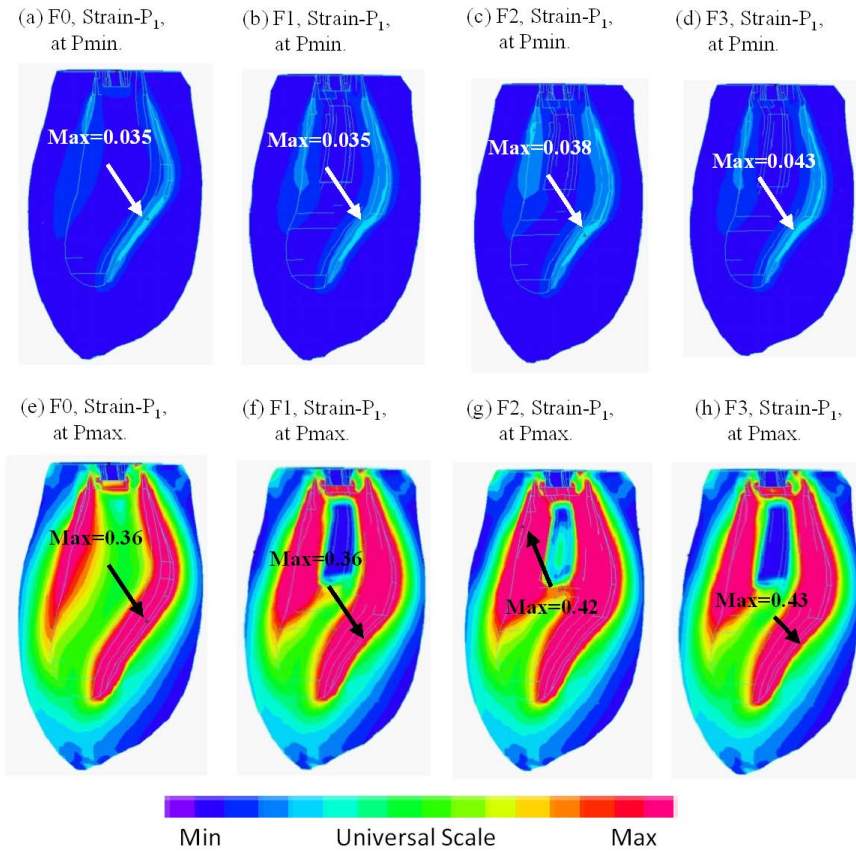


Figure 9: Model comparison: Strain- P_1 distributions obtained from the patched FSI models showing that small Strain- P_1 happened on the patch area.

Table 3: Summary of maximal Stress- P_1 /Strain- P_1 values under maximal pressure from the four models.

	F0	F1	F2	F3
Maximum of Stress- P_1 under Pmax (kPa)	19	73	75	24
Maximum of Strain- P_1 under Pmax	0.36	0.45	0.42	0.43

(P1-P5) were selected and Figures 10-11 show Stress- P_1 and Strain- P_1 tracked at those 5 locations over a cardiac cycle. Stress- P_1 at P5 (center location) from the pericardium patch (F2) was 64.4 kPa, which was about 1200% and 2700% higher than that from F1 (4.97 kPa) and F3 (2.30 kPa), respectively. Strain- P_1 at P5 from F2 was 0.0477, that was about 13 times and 16 times higher than that from F1 (0.0034) and F3 (0.0027), respectively. Stress and strain behaviors at the 5 locations can be seen in Figures 10-11 and maximal values are summarized in Table 4. Clearly Model F2 (the pericardium patch) showed the highest overall stress and strain level in the patch area.

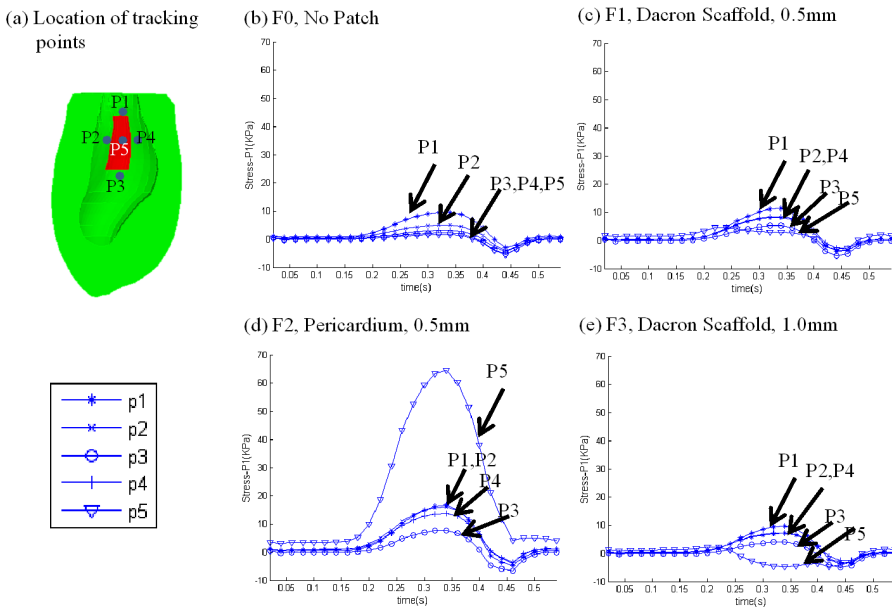


Figure 10: Maximum principal stress (Stress- P_1) variations tracked at selected tracking locations for the four models showing that stress around patch has similar results in different models but stress on the patch varied with different models.

For getting more information about the behaviors of stress/strain on the patch, we took the average of Stress- P_1 and Strain- P_1 for points on the patch in one cardiac cycle. Figure 12 gives the averaged Stress- P_1 and Strain- P_1 over a cardiac cycle showing patch material had dominant impact on stress and strain behaviors comparing with the thickness of patch. Softer material gave higher stress and strain on the patch area. Thicker patch led to lower stress and strain on the patch area but the difference was not significant.

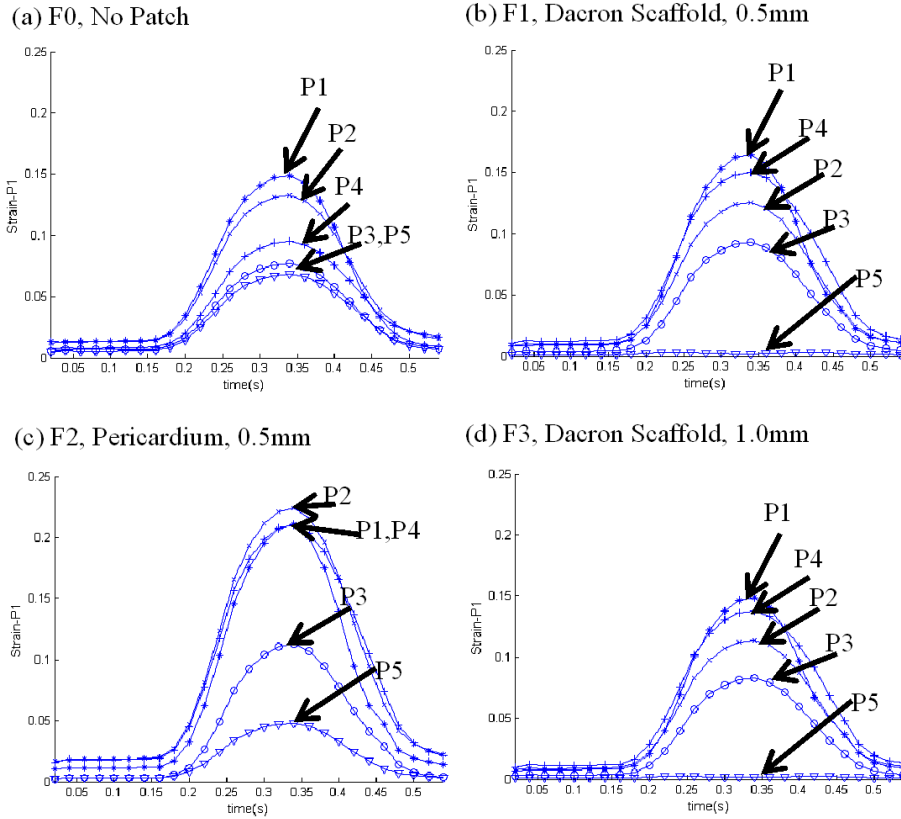


Figure 11: Maximum principal strain (Strain- P_1) variations tracked at selected tracking locations for the four models showing that strain on the patch point (P5) changed a lot in different models.

Table 4: Summary of maximal values of tracking curves at five locations from the four models.

Location	Stress- P_1 (kPa)				Strain- P_1			
	F0	F1	F2	F3	F0	F1	F2	F3
P1(below)	9.65	11.39	16.69	9.71	0.149	0.165	0.211	0.149
P2(left)	5.10	8.17	16.04	7.14	0.133	0.126	0.224	0.114
P3(top)	2.27	5.37	7.73	4.14	0.077	0.093	0.113	0.083
P4(right)	3.25	8.47	13.75	7.22	0.095	0.150	0.211	0.138
P5(center)	1.68	4.97	64.40	2.30	0.068	0.003	0.048	0.003

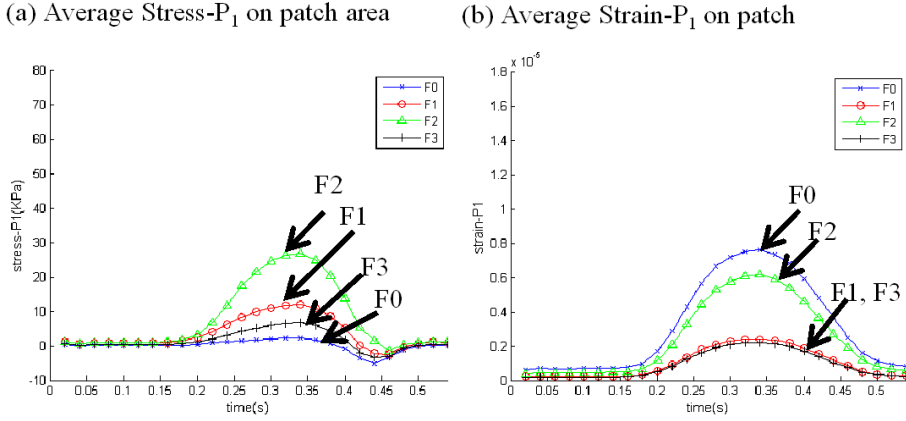


Figure 12: Averaged Stress- P_1 , Strain- P_1 on the patch in the four FSI models over a cardiac cycle. Average values show that patch material has dominant impact on the strain/stress comparing with the thickness of patch. Stiffer material patch leads to smaller values.

3.3 RV cardiac function analysis, RV volume and ejection fractions

Results from the no-patch model and three patch models were used to evaluate the effect of patches on RV function. The two common measures of RV function evaluated were stroke volume (SV) and ejection fraction (EF) defined as:

$$SV = RV \text{ End Diastolic Volume (RVEDV)} - RV \text{ End Systolic Volume (RVESV)}, \quad (13)$$

$$EF = (RVEDV - RVESV) / RVEDV. \quad (14)$$

RVEDV, RVESV, SV and EF values for F0, F1, F2 and F3 are summarized in Table 5. The results indicate that all the patch models have a higher EF value than the no-patch model. In the three patch models, F2 has the highest EF value and provide about 10% relative increase in EF (EF increase was 2.53%), F1 and F3 had 4.07% and 2.45% relative EF increase, respectively. The change was relatively small because the total patch area was only a small portion of the total RV surface area. The observation that EF values for all the three patch models were larger than no-patch model can be attributed to the fact that all the patch thickness was considerably thinner than normal myocardium.

To concentrate on the patch area and illustrate the differences among the three patch

Table 5: Stroke volume and ejection fraction comparison for four models.

Model	RVEDV(ml)	RVESV(ml)	SV(ml)	EF
F0	11.021	8.233	2.788	25.30%
F1	11.152	8.215	2.937	26.33%
F2	11.405	8.231	3.174	27.83%
F3	11.133	8.248	2.886	25.92%

Table 6: Patch area change comparisons for four models.

Model	Baseline model F0 without patch	Patch model F1 Dacron Scaffold 0.5 mm	Patch model F2 Pericardium 0.5 mm	Patch model F1 Dacron Scaffold 1 mm
RVEDPA (cm²)	3.865	3.129	3.448	3.123
RVEDPA (cm²)	3.112	3.111	3.112	3.111
Patch Area Change	0.753	0.018	0.336	0.012
Patch Area Change Fraction (%)	19.483	0.575	9.745	0.384

materials, patch area changes are summarized in Table 6 where

$$\text{RVEDPA} = \text{RV End Diastolic Patch Area}, \quad (15)$$

$$\text{RVESPA} = \text{RV End Systolic Patch Area}. \quad (16)$$

Dacron patch areas (F1 and F3) hardly changed because the scaffold material was very stiff. The pericardium patch area changed larger than the Dacron patch. Comparison between model F1 and model F3 shows that thin patch would lead to higher change in patch area.

3.4 Flow velocity has complex patterns in the ventricle

Figures 6 & 7 gave plots of the velocity and flow shear stress patterns within a cardiac cycle. Comparison of the flow results between the four FSI models indicates that the flow in different models had similar patterns but different values. Table 7 presents the peak velocity values at the tricuspid and pulmonary valves at selected time points from the four models. Flow velocity and shear stress information will be useful for detailed mechanical analysis for tissue engineering when local flow environment becomes relevant. Our results indicated that flow patterns and pressure distributions in the patched RV were similar to that in RV without patch.

Table 7: Peak velocity values at the tricuspid and pulmonary valves for selected time points from the four models.

Model	Peak Velocity During Diastole (cm/s)			Peak Velocity During Systole (cm/s)		
	Time (s)	0.02	0.24	0.30	0.40	0.44
F0	32.90	190.9	62.56	201.5	328.4	36.46
F1	33.98	201.5	71.86	233.7	354.2	36.82
F2	35.69	217.3	78.21	257.9	382.9	38.28
F3	33.61	223.3	79.62	215.6	322.2	35.73

4 Discussion

4.1 Motivation to develop myocardium tissue regeneration techniques

With the rapidly increasing number of late survivors of tetralogy of Fallot repair, surgical management of patients with right ventricular dysfunction has become a major clinical challenge. The wide variability in clinical status, extent of right ventricular dilatation, scarring, and dysfunction at the time of presentation has resulted in disparate surgical results with pulmonary valve insertion alone [16]. Del Nido and Geva et al. have proposed aggressive scar tissue trimming and RV volume remodeling to improve RV function after pulmonary valve replacement surgery [1]. Clearly, contracting myocardium would be the most desirable patch material for RV remodeling, likely leading to recovery of ventricular functions after PVR and RV remodeling surgery.

4.2 Model limitations and possible future improvements

This is our initial work to introduce fluid-structure-interactions RV/LV/Patch models to assist in choosing patch material and design and identifying optimal mechanical environment for myocardium regeneration. Several improvements can be added to our models if needed for better accuracy and applicability: a) Use medical imaging to obtain more ventricle morphology data for better model construction; b) Add more accurate valve location and mechanics into the model; c) Add subject-specific myocardium fiber orientation into our model; d) Add active contraction into our model. One way to add active contraction into our model is to introduce two separate zero-stress ventricle geometries, one for systole, and one for diastole. This is one of our future research topics.

5 Conclusions

The study is part of the collaborative effort for myocardium regeneration. It is shown that patch material properties and thickness have considerable impact on flow and stress/strain conditions in the patch area, which have direct impact for myocytes seeding, adhesion and multiplication. Combination of computational models and in vivo animal studies will help us to quantify optimal patch material properties and thickness under which optimal myocardium regeneration could be achieved. It is expected that the improved computational model for canine heart can be used as a powerful tool in the study of cell biology and tissue regeneration.

Acknowledgement: This research was supported in part by NIH-1R01-HL 089269 (del Nido, Tang, Geva). Chun Yang's research is supported in part by National Sciences Foundation of China 11171030.

References

1. del Nido, P. J. (2006) Surgical management of right ventricular dysfunction late after repair of Tetralogy of Fallot: right ventricular remodeling surgery. *Semin Thorac Cardiovasc Surg Pediatr Card Surg Annu.*, 29–34.
2. Therrien, J., Siu, S. C. & McLaughlin, P. R. (2000) Pulmonary valve replacement in adults late after repair of Tetralogy of Fallot: are we operating too late? *J. Am. Coll. Cardiol.*, 36, 1670–1675.
3. Vliegen, H. W., Van Straten, A., De Roos, A., Roest, A. A., Schoof, P. H., Zwinderman, A. H., Ottenkamp, J., Van Der Wall, E. E. & Hazekamp, M. G. (2002) Magnetic resonance imaging to assess the hemodynamic effects of pulmonary valve replacement in adults late after repair of Tetralogy of Fallot. *Circulation*, 106, 1703–1707.
4. Tang, D., Yang, C., Geva, T., Gaudette, G. & Del Nido, P. J. (2011) Multi-physics MRI-based two-layer fluid-structure interaction anisotropic models of human right and left ventricles with different patch materials: cardiac function assessment and mechanical stress analysis. *Comput Struct.*, 89, 11-12, 1059–1068.
5. Kochupura, P. V., Azeloglu, E. U., Kelly, D. J., Doronin, S. V., Badylak, S. F., Krukenkamp, I. B., Cohen, I. S. & Gaudette, G. R. (2005) Tissue-engineered myocardial patch derived from extracellular matrix provides regional mechanical function. *Circulation*, 112, I-144-I-149

6. Yang, C., Tang, D., Haber, I., Geva, T. & del Nido, P. J. (2007) In vivo MRI-based 3D FSI RV/LV models for human right ventricle and patch design for potential computer-aided surgery optimization. *Computers & Structures*, 85, 988–997.
7. Tang, D., Yang, C., Geva, T. & del Nido, P. J. (2008) Patient-specific MRI-based 3D FSI RV/LV/Patch models for pulmonary valve replacement surgery and patch optimization. *J. of Biomech. Engineering.*, 130, 4, 041010.
8. Tang, D., Yang, C., Geva, T. & del Nido, P. J. (2007) Two-layer passive/active anisotropic FSI models with fiber orientation: MRI-based patient-specific modeling of right ventricular response to pulmonary valve insertion surgery. *Molecular & Cellular Biomechanics*, 4, 3, 159–176.
9. Tang, D., Yang, C., Zheng, J., Woodard, P. K., Sicard, G. A., Saffitz, J. E. & Yuan, C. (2004) 3D MRI-based multi-component FSI models for atherosclerotic plaques a 3-D FSI model. *Ann. Biomed. Eng.*, 32, 7, 947–960.
10. Sacks, M. S. & Chuong, C. J. (1993) Biaxial mechanical properties of passive right ventricular free wall myocardium. *J. Biomech. Eng.*, 115, 202–205.
11. Humphrey, J. D. (2002) *Cardiovascular Solid Mechanics*. Springer-Verlag, New York.
12. Bathe, K. J. (2002) *Theory and Modeling Guide*. Vol. Vols. I and II. ADINAS R&D, Inc.; Watertown, MA.
13. Bathe, K. J. (1996) *Finite Element Procedures*. Prentice-Hall; Englewood Cliffs, NJ.
14. Kuehne, T., Yilmaz, S., Steendijk, P., Moore, P., Groenink, M., Saaed, M., Weber, O., Higgins, C. B., Ewert, P., Fleck, E., Nagel, E., Schulze-Neick, I. & Lange, P. (2004) Magnetic resonance imaging analysis of right ventricular pressure-volume loops: in vivo validation and clinical application in patients with pulmonary hypertension. *Circulation*, 110, 2010–2016.
15. Bathe, K. J. & Zhang, H. (2004) Finite element developments for general fluid flows with structural interactions. *Int. Journal for Numerical Methods in Engineering*, 60, 213–232.
16. Waien, S. A., Liu, P. P., Ross, B. L., Williams, W. G., Webb, G. D. & McLaughlin, P. R. (1992) Serial follow-up of adults with repaired tetralogy of Fallot. *J. Am. Coll. Cardiol.*, 20, 295-300.

